




Article

Contributions of Ammonia to High Concentrations of PM_{2.5} in an Urban Area

Junsu Park ^{1,2} , Eunhye Kim ^{3,4}, Sangmin Oh ¹ , Haeri Kim ¹, Soontae Kim ³ , Yong Pyo Kim ⁵ and Mijung Song ^{1,6,*}

- ¹ Department of Environment and Energy, Jeonbuk National University, Jeonju-si 54896, Jeollabuk-do, Korea; karmon2@naver.com (J.P.); osm3273@naver.com (S.O.); marten200@naver.com (H.K.)
 - ² Animal Environment Division, National Institute of Animal Science, 1500, WanjuGun 55365, Jeollabuk-do, Korea
 - ³ Department of Environmental Safety and Engineering, Ajou University, Suwon-si 16499, Gyeonggi-do, Korea; kiesloveeh@ajou.ac.kr (E.K.); soontaekim@ajou.ac.kr (S.K.)
 - ⁴ Emission Inventory Management Team, National Air Emission Inventory and Research Center, Cheongju 28166, Chungcheongbuk-do, Korea
 - ⁵ Department of Chemical Engineering and Materials Science, System Health & Engineering Major in Graduate School (BK21 Plus Program), Ewha Womans University, Seoul 03760, Korea; yong@ewha.ac.kr
 - ⁶ Department of Earth and Environmental Sciences, Jeonbuk National University, Jeonju-si 54896, Jeollabuk-do, Korea
- * Correspondence: mijung.song@jbnu.ac.kr; Tel.: +82-63-270-3394

Abstract: Atmospheric ammonia (NH₃) plays a critical role in PM_{2.5} pollution. Data on atmospheric NH₃ are scanty; thus, the role of NH₃ in the formation of ammonium ions (NH₄⁺) in various environments is understudied. Herein, we measured concentrations of NH₃, PM_{2.5}, and its water-soluble SO₄^{2−}, NO₃[−], and NH₄⁺ ions (SNA) at an urban site in Jeonju, South Korea from May 2019 to April 2020. During the measurement period, the average concentrations of NH₃ and PM_{2.5} were 10.5 ± 4.8 ppb and 24.0 ± 12.8 µg/m³, respectively, and SNA amounted to 4.3 ± 3.1, 4.4 ± 4.9, and 1.6 ± 1.8 µg/m³, respectively. A three-dimensional photochemical model analysis revealed that a major portion of NH₃, more than 88%, originated from Korea. The enhancement of the ammonium-to-total ratio of NH₃, NH_x (NHR = [NH₄⁺]/[NH₄⁺] + [NH₃]) was observed up to ~0.61 during the increase of PM_{2.5} concentration (PM_{2.5} ≥ 25 µg/m³) under low temperature and high relative humidity conditions, particularly in winter. The PM_{2.5} and SNA concentrations increased exponentially as NHR increased, indicating that NH₃ contributed significantly to SNA formation by gas-to-particle conversion. Our study provided experimental evidence that atmospheric NH₃ in the urban area significantly contributed to SNA formation through gas-to-particle conversion during PM_{2.5} pollution episodes.

Keywords: ammonia; ammonium nitrate; PM_{2.5}; aerosol pollution; urban



Citation: Park, J.; Kim, E.; Oh, S.; Kim, H.; Kim, S.; Kim, Y.P.; Song, M. Contributions of Ammonia to High Concentrations of PM_{2.5} in an Urban Area. *Atmosphere* **2021**, *12*, 1676. <https://doi.org/10.3390/atmos12121676>

Academic Editors: Theodora Nah, Shaojie Song and Zongbo Shi

Received: 19 November 2021

Accepted: 11 December 2021

Published: 14 December 2021

Publisher's Note: MDPI stays neutral with regard to jurisdictional claims in published maps and institutional affiliations.



Copyright: © 2021 by the authors. Licensee MDPI, Basel, Switzerland. This article is an open access article distributed under the terms and conditions of the Creative Commons Attribution (CC BY) license (<https://creativecommons.org/licenses/by/4.0/>).

1. Introduction

Global emissions of NH₃ have annually increased from an estimated 1.9 Tg in the 1960s to 16.7 Tg in 2010 [1]. Reports have indicated that the main source of atmospheric NH₃ at the global scale is agricultural activities involving livestock, fertilizers, soil, and crops [2–5]; these activities accounted for approximately 60% of the total NH₃ emitted from Asia in the 2000s [1]. NH₃ is important because it can contribute to the acidification of ecosystems [6,7]. Moreover, it plays a critical role in chemical reactions in the atmosphere, where its conversion to particulate ammonium can lead to high concentrations of particulate matter [8–14]. These particulate ammonium can influence air quality, visibility, and human health [15–17].

Field measurements have shown that concentrations of atmospheric NH₃ generally vary depending on the season and location [9,18–27]. NH₃ concentrations are temperature-dependent; they increase in summer and decrease in winter [9,20]. For example, an average ambient NH₃ concentration of ~36.2 ppb, with variations ranging from ~73.9 ppb in July to

~13.5 ppb in September, was detected in the Northern Plains of China in 2013 [8]. Only a few studies have been conducted in Korea, which showed the average NH_3 concentration in Seoul of ~6.0 ppb from 1996 to 1997 and ~11.0 ppb from 2010 to 2011 [23,27], and 10.5 ppb in Jeon-ju from 2019 to 2020, with higher concentrations occurring during the summer [19].

NH_3 in the atmosphere can react with acidic species, such as sulfuric acid (H_2SO_4), nitric acid (HNO_3), and hydrochloric acid (HCl), which lead to the production of secondary inorganic aerosols (SIAs) including ammonium sulfate $((\text{NH}_4)_2\text{SO}_4)$, ammonium nitrate (NH_4NO_3), and ammonium chloride (NH_4Cl) [28,29]. Previous studies have shown that these SIAs can account for up to ~70% of the mass of $\text{PM}_{2.5}$, depending on the location and season [30–34]. Moreover, recent studies have shown that high conversion ratios of ammonium from the gas to particle phase can significantly promote high $\text{PM}_{2.5}$ concentration [8,9,25,35–39]. In rural areas of Shanghai, China, $\text{PM}_{2.5}$ concentrations were found to be influenced by secondary NH_4^+ from NH_3 at a conversion ratio of up to ~0.8 during periods of high $\text{PM}_{2.5}$ pollution in October 2013 [9]. In Delhi, India, the conversion ratio from NH_3 to NH_4^+ increased up to ~0.6 during $\text{PM}_{2.5}$ pollution episodes from 2013 to 2015 [36]. Increases of SIAs following increasing water content of aerosols result in various aqueous phase reactions and high concentration of $\text{PM}_{2.5}$ [40–42]. Although atmospheric NH_3 is one of the key species for the formation of SIAs, which cause aerosol pollution, studies on evaluations of the impacts of NH_3 on the formation of $\text{PM}_{2.5}$ are still limited. In addition, characteristics of atmospheric NH_3 and its impact on $\text{PM}_{2.5}$ pollution are scarce in urban areas.

In this study, atmospheric NH_3 and water-soluble ions, including SO_4^{2-} , NO_3^- , and NH_4^+ (SNA) concentrations were measured over one year from May 2019 to April 2020 in an urban area, Samcheon-dong, Jeonju, South Korea. Using the dataset, we explored how the ambient NH_3 contributes to high concentrations of $\text{PM}_{2.5}$. Moreover, we applied a three-dimensional photochemical model to identify the origin of the ambient NH_3 . Altogether, our results provide a more comprehensive understanding of the gas-to-particle conversion process in the atmosphere and the role of NH_3 in the formation of aerosol pollution.

2. Materials and Methods

2.1. Monitoring Site

The concentrations of NH_3 and SIAs in $\text{PM}_{2.5}$ were measured from 4 May 2019 to 15 April 2020 at a monitoring station in Samchon-dong, Jeonju, Jeollabuk-do, South Korea ($35^\circ 47' 56.4''$ N, $127^\circ 7' 19.2''$ E) (Figure 1). The monitoring site can be considered as a representative urban site for Jeollabuk-do because the area is surrounded by residential clusters, business buildings, and roads. It is located ~50 km from agricultural areas consisting of large- and small-scale livestock farms (pigs, cows, and chickens) and other types of farmlands, ~75 km from the Yellow Sea, ~190 km from Busan, and ~200 km from Seoul.

2.2. Measurements

The method of NH_3 measurements has been previously described by Park et al. [19]. Briefly, atmospheric NH_3 concentrations were measured with cavity ring-down spectroscopy (CRDS) (Picarro Inc., model G2103, Santa Clara, CA, USA) on a 1 s basis from 4 May 2019 to 15 April 2020, and the 1-h-averaged data were used for the analyses. The NH_3 analyzer has an average precision of 0.03 ppb for 300 s, with a response time of less than 1 s and a detection limit below 0.09 ppb [43]. Additionally, the analyzer has a low drift value of 0.15 ppb over 72 h [43]. Theoretically, atmospheric NH_3 absorbs light of a characteristic wavelength from within the cavity; when the laser is turned off, the concentration can be calculated using the attenuation curves that disappear. No additional external calibration is required, according to the manual for the Model G-2103 CRDS analyzer [44]. However, in this study, calibration was conducted to confirm the performance of the analyzer by using a mixture of standard NH_3 (11.9 ppm, Airkorea, Korea) and N_2 gas. The calibration was repeated three times with four points at 25, 20, 15, and 5 ppb, and the resulting R^2 was 0.997 (Figure S1). During the measurement period, perfluoroalkoxy (PFA) tubing (internal

diameter 4 mm) was used for the inlet, and the inlet length was as short as possible (~1.5 m) to limit the residence time to shorter than 1 s during the measurement period [8].

PM_{2.5} was collected on Teflon filters (PTFE, R2PJ047, PALL, New York, USA) over a 24-h period from 09:00 am to 09:00 am at a flow rate of 16.67 L/min using a sequential low volume sampler (APM, PMS-104, Bucheon, Korea) at the monitoring site. A total of 118 PM_{2.5} filters were collected during the measurement period (Table S1). The mass concentration of PM_{2.5} was determined using the method recommended by the USA. Environmental Protection Agency (EPA) (Compendium of Methods for the Determination of Inorganic Compounds in Ambient Air, Methods), (EPA, <https://www.epa.gov>) (accessed on 15 September 2021). The concentrations of ion species such as NO₃[−], SO₄^{2−}, and NH₄⁺, as well as minor ions in the PM_{2.5}, were analyzed by ion chromatography (AQUION, Thermo Scientific, Massachusetts, USA).

Hourly averaged meteorological parameters of temperature, relative humidity (RH), wind speed, and wind direction were collected from the Jeollabuk-do Institute of Health and Environment Research. The hourly average temperature during the measurement period was 13.6 ± 9.5 °C, and the relative humidity was 67.6 ± 18.6%. To reduce the uncertainties from measurements and instruments during high-precipitation events [45,46], data were excluded from the analyses when the hourly amount of precipitation exceeded 5 mm. These excluded data (~10.5% of the original measured NH₃ data) were mostly from July–August and September (~10.3% of the original measured NH₃ data) due to the monsoon and frequent occurrence of typhoons, respectively.

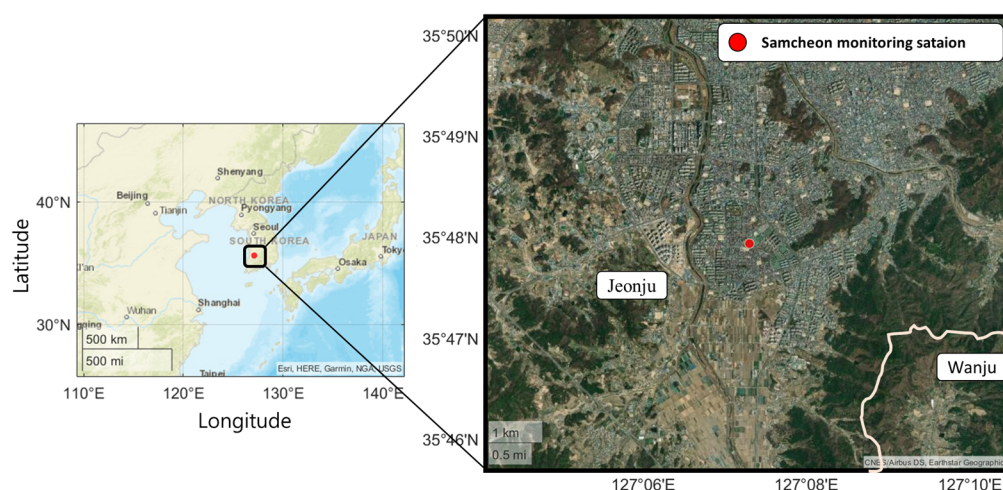


Figure 1. Map of the measurement site in Jeonju, South Korea (35°47′56.4″ N, 127°7′19.2″ E).

2.3. Modelling

Identifying the origins of the NH₃ is challenging because the airborne NH₃ concentration is affected by various physical and chemical processes, including emission, transport, deposition, and chemical transformation. In this study, we simulated NH₃ and NH₄⁺ concentrations in Northeast Asia using the community multiscale air quality (CMAQ) model version 4.7.1 [47]. It is a three-dimensional photochemical model. To operate CMAQ, the meteorological inputs were prepared using Weather Research and Forecasting (WRF) version 3.5.1 [48] with final operational global analysis data. The Sparse Matrix Operator Kernel Emission (SMOKE; version 3.1) [49] was applied to process the KORUSv5 emissions inventory [50,51] for regional emissions, excluding South Korea. For South Korea, CAPSS 2016, developed and released by the National Air Emission Inventory and Research Center (NAIR), was utilized [52].

In the WRF-SMOKE-CMAQ simulation, the brute force method (BFM) was applied to identify the relative contribution of NH₃ and NH₄⁺ from China and South Korea to the downwind area. The BFM estimates the sensitivity of pollutant concentrations to change in targeted emissions [53]. Kim et al. [54] showed that the estimated contributions using

BFM with different emission perturbation regions or rates were not identical, showing non-linearity of responses. Considering that a 100% emission reduction for a region may severely change the chemical condition, in this study, we calculated the sensitivity of NH_x (total ammonia; $[\text{NH}_4^+] + [\text{NH}_3]$) concentrations in South Korea to Chinese NH_3 emissions through 50% reduced Chinese NH_3 emissions using Equation (1) [55]. The emission perturbation rate has been used in previous air quality modeling studies over the region [56–58]. We assumed that the change of NH_x concentrations in South Korea to the NH_3 emission perturbations in China shows a low nonlinear response based on a previous NH_3 sensitivity conducted by Kim et al. [55].

$$\text{Sensitivity } (\mu\text{g}/\text{m}^3) = C_B - C_{C,50\%} \quad (1)$$

where C_B is the NH_3 (or NH_x) concentration simulated using the base run, $C_{C,50\%}$ is the NH_3 (or NH_x) concentration simulated using a 50% reduction in Chinese NH_3 emissions, and $\Delta E_{50\%}$ is the emission perturbation rate (0.5 in this study). Then, the zero-out contribution (ZOC) of Chinese NH_3 emissions to NH_3 concentrations in South Korea was calculated by dividing the NH_3 sensitivity by the perturbation rate (0.5 in this study) [56,58] as shown in Equation (2). Additionally, the difference between the NH_3 concentration in the base run and the ZOC of Chinese NH_3 in the downwind area was considered as the ZOC of South Korea.

$$\text{NH}_3 \text{ ZOC } (\mu\text{g}/\text{m}^3) = \frac{\text{NH}_3 \text{ Sensitivity}}{\Delta E_{50\%}} \quad (2)$$

3. Results and Discussion

3.1. Characteristics of Atmospheric NH_3 in Urban Area

During the entire measurement period at the urban site, the hourly averaged concentration of atmospheric NH_3 was 10.5 ± 4.8 ppb, ranging from 2.0 ppb to 54.5 ppb. These atmospheric NH_3 concentrations are comparable to those measured in other regions (Table 1). The NH_3 level in Jeonju was similar in Seoul in 2010–2011 [23], which was higher than that of the Shanghai urban area in China in 2013 [9]. Moreover, the NH_3 concentration in Jeonju was higher than that of Osaka, Japan, and Ho Chi Minh, Vietnam in 2015, also in Asia [22]. Further, the NH_3 concentration in the urban area was up to 3–4 times higher than that of North America and Europe (Table 1) [24,25,59].

Table 1. Concentrations of atmospheric NH_3 in various environments.

Location	Period	Type	NH_3 (Mean \pm Std) (Unit: ppb)	Reference
Jeonju, Korea	May 2019–April 2020	Urban	10.5 ± 4.8	This study
Seoul, Korea	October 1996–September 1997 September 2010–August 2011	Urban	6.0 10.9 ± 4.25	Lee et al., 1999 [27] Phan et al., 2013 [23]
Shanghai, China	July 2013–September 2014	Urban Rural Industrial	6.2 ± 4.6 12.4 ± 9.1 17.6 ± 9	Wang et al., 2015 [9]
Osaka, Japan	February–March 2015 July–September 2015	Urban	1.98 ± 0.93 4.21 ± 2.30	Huy et al., 2017 [22]
New Delhi, India	January 2013–December 2015	Urban	19.6 ± 3.5	Saraswati et al., 2019 [36]
Ho Chi Minh, Vietnam	May 2015–June 2015	Urban	8.34 ± 2.47	Huy et al., 2017 [22]
Ontario, Canada	March 2010–March 2011	Rural	4.7	Zbieranowski and Aherne 2012 [59]
Barcelona, Spain	May 2011–September 2011 May 2011–June 2011	Urban background Urban	2.9 ± 1.3 7.5 ± 2.8	Pandolfi et al., 2012 [25]
Houston, TX, USA	February 2010–March 2010 August 2010–September 2010	Urban	2.4 ± 1.2 3.1 ± 2.9	Gong et al., 2011 [24]

Shown in Figure 2 is the seasonal diurnal variation of the atmospheric NH_3 observed at the urban site. In spring and summer, the diurnal variation of the ambient NH_3 concentration was low, from 00:00 to 12:00 local time, and then the concentration increased and reached a maximum concentration of more than ~14 ppb at 20:00. Previous studies reported that such variations, with high concentrations observed in late afternoon, are caused by NH_3 transport to urban area from the vicinity of rural areas by agricultural sources, expansion of a planetary boundary layer, and wind directions [60,61]. This could explain the high concentration in the study site, which is surrounded by agricultural lands (rice fields, and large and small livestock farms) ~10 km to the west and southwest (Figure S2). A recent study simultaneously measured atmospheric NH_3 concentration from rural and urban areas, which are close to the present study site, and showed that the NH_3 concentrations at both sites (rural and urban areas) were significantly higher in summer, particularly in June, than in other seasons [62]. When the highest atmospheric NH_3 concentrations occurred in June in the urban area, elevated NH_3 concentrations were also observed in the adjacent rural area [62]. They suggested that the enhanced ambient NH_3 concentrations observed in the urban area were influenced by high NH_3 concentrations from the rural area located to the west [62]. Contrastingly, bimodal peaks in the morning and late afternoon determined in autumn and winter were likely due to the impact of traffic in the urban areas.

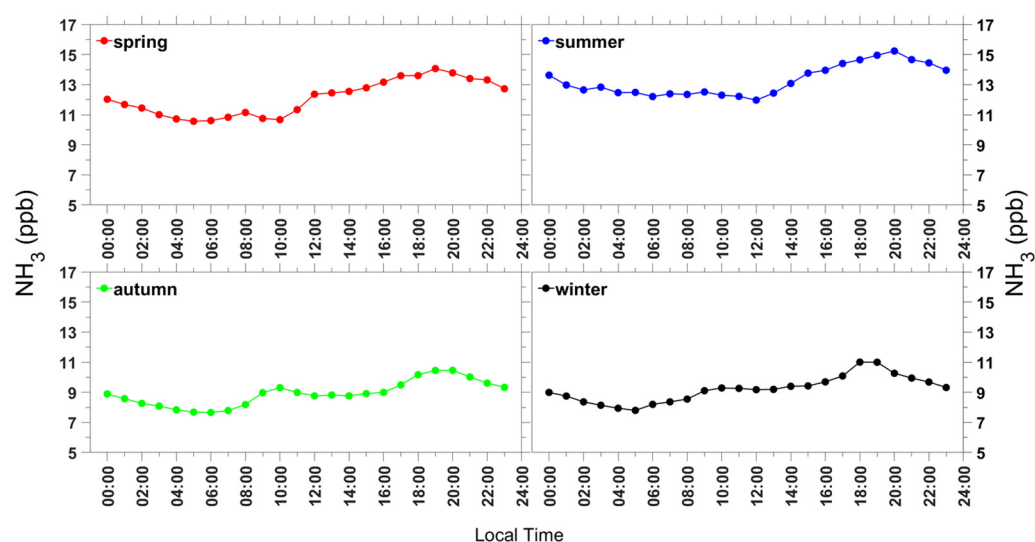


Figure 2. Seasonality of hourly averaged diurnal variations of atmospheric NH_3 at the monitoring station during 2019–2020. Spring: May 2019, and March and April 2020. Summer: June and August 2019. Autumn: September–November 2019. Winter: December 2019 to February 2020.

Seasonally, the NH_3 concentration in Jeonju was observed as follows: summer (13.3 ± 5.8 ppb) > spring (12.1 ± 5.1 ppb) > winter (9.2 ± 4.3 ppb) > autumn (8.9 ± 3.1 ppb) (Figure 3). In this study, the NH_3 concentration showed a strong correlation with ambient temperature (Figure S3). The atmospheric NH_3 concentration in the urban site was enhanced as temperature was increased, which is consistent with previous studies [8,9,19,20,37,38,62]. However, the concentrations decreased when the temperature was above 30 °C (Figure S3), because of the wet deposition and removal effects that occur in monsoon (Figure S4) [9,19,36].

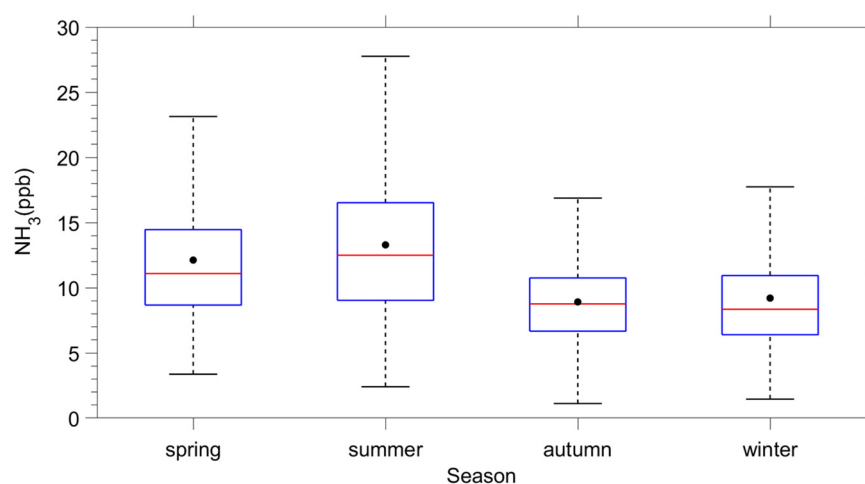


Figure 3. Seasonal NH_3 concentrations at the monitoring site. Box lines represent the 75th quartile and the 25th quartile, and whiskers represent the minimum and maximum concentration values, excluding outliers. The black dot indicates average concentration of NH_3 for each season, and the red line indicates median concentration.

3.2. Contribution of NH_3 to $\text{PM}_{2.5}$ Pollution

To explore the effects of NH_3 on aerosol pollution, which have never been studied in Korea through field measurements, we measured $\text{PM}_{2.5}$ and its water-soluble ions, and investigated how NH_3 contributes to NH_4^+ formation and the production of $\text{PM}_{2.5}$. Throughout the measurement period, the monthly average $\text{PM}_{2.5}$ concentration was $24.0 \pm 12.8 \mu\text{g}/\text{m}^3$, and NO_3^- was the most abundant ($4.4 \pm 4.9 \mu\text{g}/\text{m}^3$), followed by SO_4^{2-} ($4.3 \pm 3.1 \mu\text{g}/\text{m}^3$) and NH_4^+ ($1.6 \pm 1.8 \mu\text{g}/\text{m}^3$) in the $\text{PM}_{2.5}$ (Figure 4b,c, Table S1). The NO_3^- in the $\text{PM}_{2.5}$ was significantly enhanced in winter time. Previous studies also reported that $\text{PM}_{2.5}$ concentrations were elevated, particularly in winter, with a remarkable increase in the NO_3^- concentrations at the measurement site during winter [63–66]. In particular, in January, high concentrations of $\text{PM}_{2.5}$ were observed, with a monthly average of $38.1 \pm 20.3 \mu\text{g}/\text{m}^3$ (Table S1), and an average NO_3^- concentration of $11.8 \mu\text{g}/\text{m}^3$ (Figure S5).

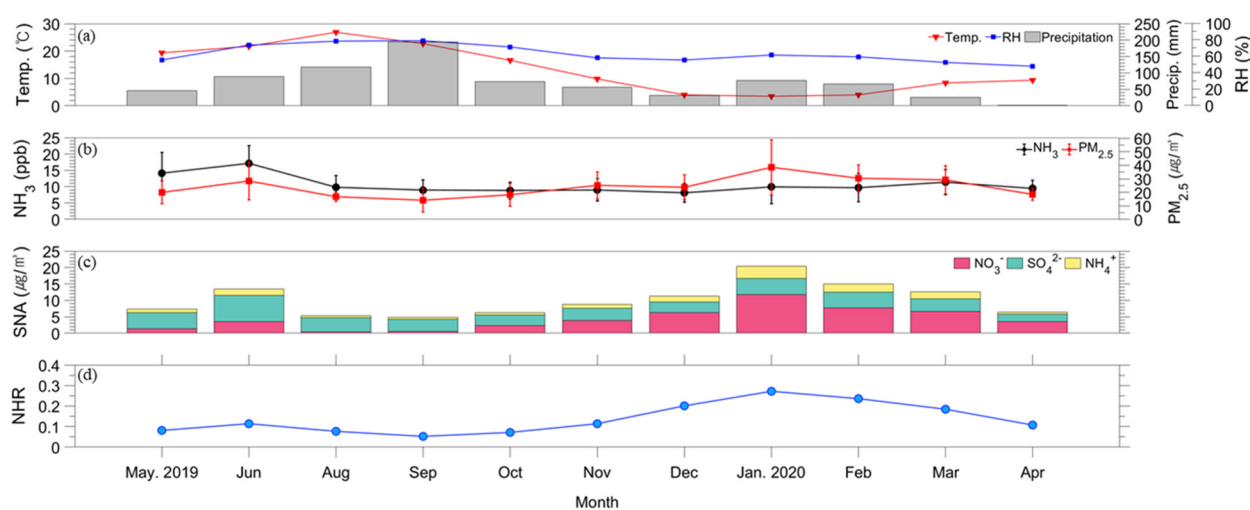


Figure 4. Monthly variations in (a) meteorological parameters, (b) NH_3 and $\text{PM}_{2.5}$ concentrations, (c) SO_4^{2-} , NO_3^- , and NH_4^+ (SNA) concentrations in $\text{PM}_{2.5}$, and (d) the ratio of NH_4^+ to total NH_3 (NHR) from May 2019 to April 2020.

In this study, $\text{PM}_{2.5}$ pollution was defined as a daily average of $\text{PM}_{2.5} \geq 25 \mu\text{g}/\text{m}^3$, based on the daily mean $\text{PM}_{2.5}$ guideline value recommended by the World Health Or-

ganization [67]. During the entire period, 47 d (spring: 13 d, summer: 6 d, autumn: 10 d, and winter: 18 d) out of a total of 118 d showed $PM_{2.5}$ pollution. Figure 5 presents a comparison of the SNA concentrations, NH_3 , and the ratio of NH_4^+ to total ammonia, NH_x (where $NHR = [NH_4^+]/([NH_4^+] + [NH_3])$) [68], for clean days ($PM_{2.5} < 25 \mu g/m^3$) versus polluted days ($PM_{2.5} \geq 25 \mu g/m^3$). On the polluted days, the NO_3^- and NH_4^+ mass fraction significantly increased to 46% and 18%, respectively, while the SO_4^{2-} fraction was reduced to 36% in the SNA fraction (Figure 5a). The NH_3 concentration was slightly higher (12.6 ppb) during $PM_{2.5}$ pollution than during clean days (10.7 ppb) (Figure 5b). Moreover, on the $PM_{2.5}$ pollution, the daily average NHR increased dramatically to 0.24 (Figure 5c), with a maximum daily ratio of 0.61 in January (Figure S5). It was comparable with the NHR of only 0.06 during the clean days.

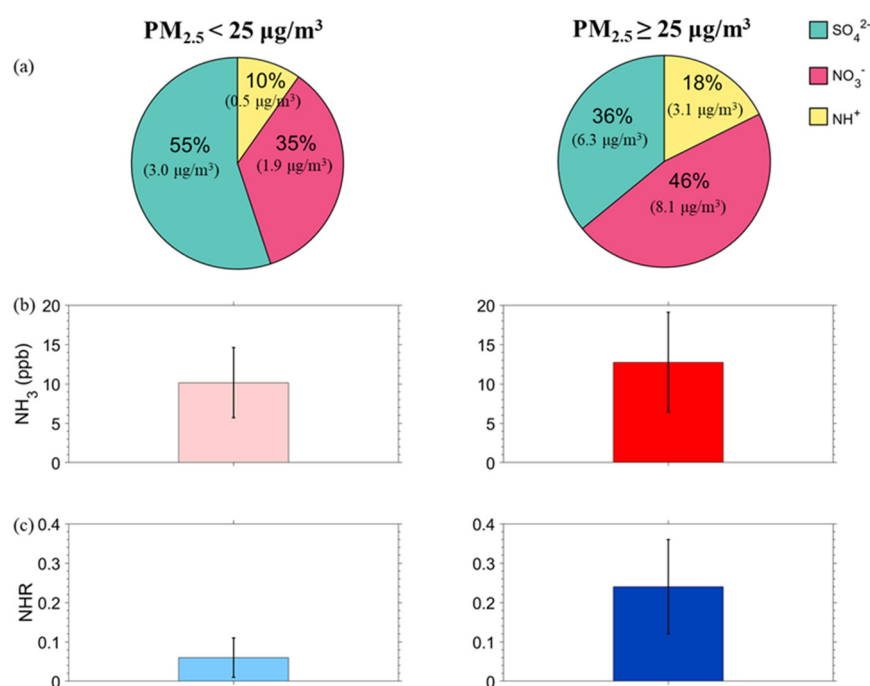


Figure 5. Comparisons of (a) SO_4^{2-} , NO_3^- , and NH_4^+ of $PM_{2.5}$, (b) NH_3 concentrations, and (c) the ratio of NH_4^+ to total NH_3 (NHR) on clean ($PM_{2.5} < 25 \mu g/m^3$) versus polluted ($PM_{2.5} \geq 25 \mu g/m^3$) days.

Illustrated in Figure 6a is the relationship between NHR and NH_3 on $PM_{2.5}$ pollution. The NHR was inversely proportional to the atmospheric NH_3 concentrations (Figure 6a), and the atmospheric NH_3 decreased as the NHR increased. These data reflect the inter-conversion between atmospheric gases and particles [9], thus, suggesting that NH_3 was converted to NH_4^+ on $PM_{2.5}$ pollution, resulting in high $PM_{2.5}$ concentration. Moreover, as the NHR increased, the $PM_{2.5}$ and SNA concentrations increased exponentially with R^2 values of 0.49 and 0.73, respectively (Figure 6b). This indicates that the increase in $PM_{2.5}$ concentration was facilitated by the reactions of gaseous NH_3 with acidic species that converted the NH_3 to particulate NH_4^+ [8,9,36].

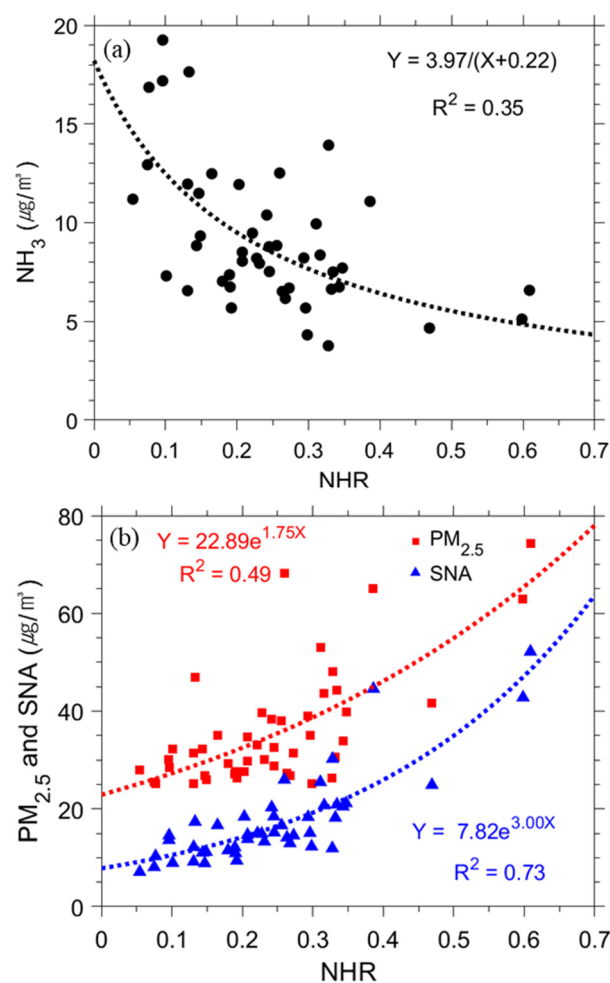


Figure 6. Relationship between the daily average ratio of NH_4^+ to total NH_3 (NHR) and (a) NH_3 concentrations, and (b) daily average $\text{PM}_{2.5}$ and SO_4^{2-} , NO_3^- , and NH_4^+ (SNA) concentrations during $\text{PM}_{2.5}$ pollution days ($\text{PM}_{2.5} \geq 25 \mu\text{g}/\text{m}^3$).

NH_3 is considered to be neutralized by sulfuric acid to form $(\text{NH}_4)_2\text{SO}_4$, and then the excess NH_3 reacts with other gaseous acidic species (i.e., HNO_3 and HCl) to form NH_4NO_3 and NH_4Cl [69]. Sung et al. [18] measured NH_3 , NO_3^- , and HNO_3 at the same urban site from 2009 to 2018 (average NH_3 : $\sim 7.8 \mu\text{g}/\text{m}^3$, NO_3^- : $\sim 3.0 \mu\text{g}/\text{m}^3$, and HNO_3 : $\sim 1.7 \mu\text{g}/\text{m}^3$) and reported that the urban area was under NH_3 -rich conditions based on the calculation of adjusted gas ratio of ~ 4 , $\text{AdjGR} = ([\text{NH}_3] + [\text{NO}_3^-])/([\text{NO}_3^-] + [\text{HNO}_3])$ [70]. This indicates that, in the urban site, NH_3 could be enough to form $(\text{NH}_4)_2\text{SO}_4$, and then the excess NH_3 could react with other gaseous acidic species to form NH_4NO_3 and NH_4Cl . In this study, based on the molar ratio of $([\text{NO}_3^-]/[\text{SO}_4^{2-}])/([\text{NH}_4^+]/[\text{SO}_4^{2-}])$, NH_4^+ -rich conditions were observed (Figure S6), again suggesting NH_4NO_3 formation during the SIA formation. NH_4NO_3 is a semi-volatile species; thus, it can exist in different phase states depending on the temperature and humidity [69]. As shown in Figures 5c and 7, a high NHR (>0.3) was found under NH_4^+ -rich, low temperature ($7.9 \pm 7.6^\circ\text{C}$) and high RH ($71.7 \pm 7.0\%$) conditions, which are the conditions of higher deliquescence RH of NH_4NO_3 [71]. These data indicate that in the study site, NH_4NO_3 was likely present in mainly the aqueous phase.

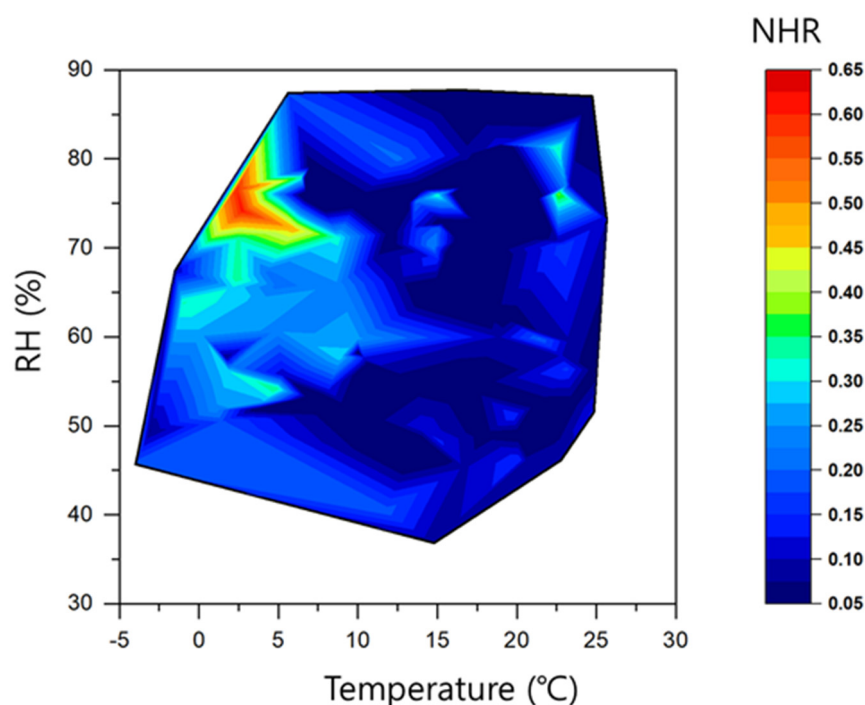


Figure 7. Daily average conversion ratios of NH_3 to NH_4^+ (NHR) as a function of temperature and relative humidity (RH) during the entire measurement period.

3.3. Origin of Total NH_3

To examine the origin of NH_3 during the measurement period, we used air quality simulation with the photochemical model. The simulated NH_3 and NH_4^+ were evaluated with the observations (Figures S7–S9 and Figure 2). The simulated NH_4^+ concentrations agreed well with the observations in the urban site. Moreover, the simulated NH_3 concentrations were overestimated by 2–6 ppb for spring, autumn, and winter in the site, which can be attributable to the uncertainty in the NH_3 emissions inventory [72].

Figure 8 shows the monthly ZOC of Chinese NH_3 emissions in Northeast Asia. The ZOC averaged over China was as high as ~ 5.3 ppb. For South Korea, however, the ZOC was as low as ~ 0.5 ppb, except during spring, when NH_3 emissions increased due to agricultural activities. It is known that transboundary transport of air pollutants from China to South Korea increases during spring compared to the other seasons [73,74]. However, the calculations yielded an NH_3 concentration of just ~ 2 ppb, which is significantly lower than the measured value during spring (~ 12 ppb) (Figure 3). This suggests that domestic influences remain strong even during the spring.

Figure 9 shows the simulated monthly NH_3 concentrations and the relative contributions of NH_3 emissions released from China and South Korea, respectively, in Samcheon-dong, South Korea. NH_x was also added because NH_3 can be converted into NH_4^+ during the long-range transport. During the study period, the relative NH_3 contributions from South Korea were dominant, ranging from 88% to 99%, despite the uncertainties that still existed in the simulation results associated with the input emissions and meteorology data. This is because most NH_3 originating from China is converted into NH_4^+ after the long-range transport, considering the short residence time of NH_3 in the atmosphere (one day or less) [75,76]. Although the simulations overestimated NH_3 concentrations in Samcheon-dong (Figure S8), they clearly confirmed that most NH_3 originated from South Korea, rather than China, during the measurement period.

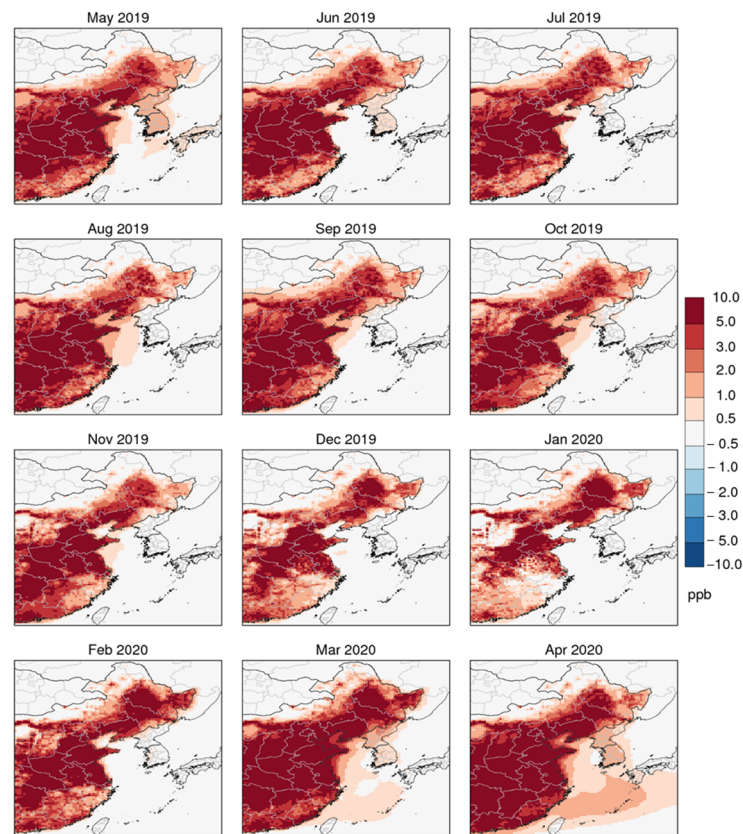


Figure 8. Simulated monthly NH_3 zero-out contributions of Chinese NH_3 emissions in Northeast Asia from May 2019 to April 2020. The darker red color represents the higher Chinese NH_3 emission impacts.

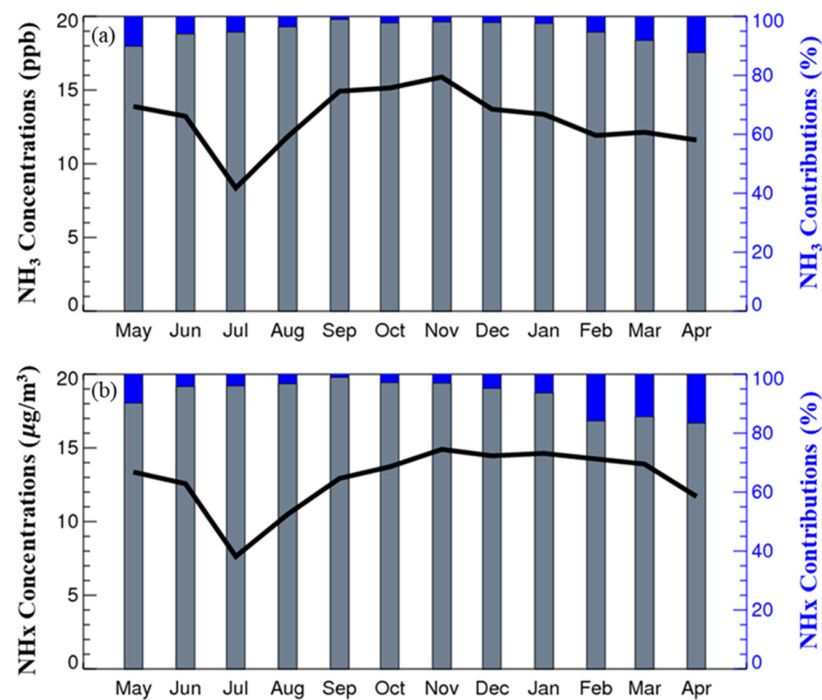


Figure 9. Simulated monthly (a) NH_3 and (b) total ammonia (NH_x) concentrations (black line) and its relative contributions (blue and gray bars) in Samcheon-dong, Korea. The blue bar represents the contribution of NH_3 and NH_x emissions in China and the gray bar represents the contribution from South Korea.

4. Conclusions

In this study, we measured the concentrations of NH_3 , $\text{PM}_{2.5}$, and its water-soluble SNA to determine the effect of NH_3 on $\text{PM}_{2.5}$ pollution at an urban area, Jeonju, South Korea from May 2019 to April 2020. During the entire period, the hourly average concentration of atmospheric NH_3 was 10.5 ± 4.8 ppb and the daily average concentration of $\text{PM}_{2.5}$ was 24.0 ± 12.8 $\mu\text{g}/\text{m}^3$ with 4.4 ± 4.9 $\mu\text{g}/\text{m}^3$ for NO_3^- , 4.3 ± 3.1 $\mu\text{g}/\text{m}^3$ for SO_4^{2-} , and 1.6 ± 1.8 $\mu\text{g}/\text{m}^3$ for NH_4^+ . Seasonal variations showed that the atmospheric NH_3 was enhanced in summer, while the $\text{PM}_{2.5}$ was increased in winter at the monitoring site. Further, when the level of atmospheric NH_3 enhanced, the concentration showed a late afternoon peak due to the influence of nearby rural areas by agricultural activities. This was evident in spring and summer; on the other hand, in winter, the two peaked during high traffic times.

During $\text{PM}_{2.5}$ pollution episodes (daily $\text{PM}_{2.5}$ average ≥ 25 $\mu\text{g}/\text{m}^3$), we observed a remarkable increase in the fraction of NH_4^+ and NO_3^- in $\text{PM}_{2.5}$. In addition, the daily average NHR increased dramatically to 0.24 (with a maximum ratio of ~ 0.61 in January) when high $\text{PM}_{2.5}$ concentration was observed. This was comparable to the result of the NHR-value of 0.06 for clean days ($\text{PM}_{2.5} < 25$ $\mu\text{g}/\text{m}^3$). We also observed an inversely proportional correlation between the NHR and NH_3 , and a strong positive exponential correlation between the NHR and $\text{PM}_{2.5}$ and SNA, suggesting that NH_3 contributed significantly to SNA formation by gas-to-particle conversion. To explore the origin of the NH_3 at the monitoring site, we performed three-dimensional photochemical models using CMAQ and BFM. The modeling results showed that most of the NH_3 originated from South Korea, rather than China, during the studied period. The simulations proved that most NH_3 originated from South Korea, rather than China, during the measurement period. Overall, our results provided an in-depth understanding of the chemistry and origin of PM precursors and aerosol pollution in the atmosphere. This knowledge can further contribute to the development of effective air quality improvement strategies, such as regulation policies for air pollutants.

Supplementary Materials: The following are available online at <https://www.mdpi.com/article/10.3390/atmos12121676/s1>, Figure S1: Calibration of the NH_3 analyzer using a diluted standard gas mixture of NH_3 and N_2 . Figure S2: A result of polar plot during the measuring period in Jeonju. Figure S3: Relationship between hourly NH_3 concentrations and ambient temperature at the Samcheon-dong monitoring station during May 2019 to April 2020. Figure S4: Hourly averaged concentration of NH_3 versus the precipitation per hour during the measuring period (temperature > 30 °C). Figure S5: Monthly variation in (a) temperature and the ratio of NH_4^+ to total NH_3 (NHR) and (b) concentrations of NH_3 , SNA, and $\text{PM}_{2.5}$ at the monitoring site in January 2020. Figure S6: NO_3^- to SO_4^{2-} molar ratio and NH_4^+ to SO_4^{2-} molar ratio used for the analysis of NH_4^+ conditions during polluted periods. Figure S7: Cluster analysis for 72 h backward trajectories at the monitoring site from May 2019 to April 2020. Figure S8: Seasonally observed (left) and simulated (right) ammonia (NH_3) concentrations in Samcheon-dong. Figure S9: Time series for the observed and simulated NH_4^+ concentrations in the six supersites (Baengnyeong, Seoul, Daejeon, Gwangju, Jeju, and Ulsan) in South Korea from May 2019 to April 2020. Table S1: Monthly average concentrations of $\text{PM}_{2.5}$ and its ionic species, and NH_3 , and meteorological conditions in Jeonju from May 2019 to April 2020. Table S2: Model performance evaluation for NH_4^+ concentrations in the six supersites (Baengnyeong, Seoul, Daejeon, Gwangju, Jeju, and Ulsan) in South Korea from May 2019 to April 2020.

Author Contributions: M.S. designed this study. J.P., S.O., H.K. and M.S. conducted field measurements and analyzed the data. E.K. and S.K. calculated model predictions and wrote the section. M.S. and J.P. prepared the manuscript with contributions of E.K., H.K., S.K., Y.P.K. and S.O. All authors have read and agreed to the published version of the manuscript.

Funding: This Research was supported by the Technology Development Program to Solve Climate Changes of the National Research Foundation (NRF) funded by the Korea government (MSIT) (NRF-2019M1A2A2103956), and Cooperative Research Program for Agriculture Science and Technology Development (PJ014248022021) funded by the Rural Development Administration, Republic of Korea.

Institutional Review Board Statement: Not applicable.

Informed Consent Statement: Not applicable.

Data Availability Statement: The publicly available Hybrid Single-Particle Lagrangian Integrated Trajectory (HYSPPLIT) model can be found at <https://www.ready.noaa.gov> (accessed on 1 May 2021) and run either online or offline. The data can be found data from the link: <ftp://arlftp.arl.hq.noaa.gov/pub/archives/gdas1/> (accessed on 1 May 2021). In this study, the PM_{2.5} mass concentration analysis method used the methodology provided by EPA, which can be found from the link: <https://www.epa.gov/amtic/compendium-methods-determination-inorganic-compounds-ambient-air> (accessed on 15 November 2021).

Acknowledgments: Mijung Song would like to thank Jaeyoun Ryoo for providing meteorological condition data.

Conflicts of Interest: The authors declare no conflict of interest.

References

- Xu, R.; Tian, H.; Pan, S.; Prior, S.A.; Feng, Y.; Batchelor, W.D.; Chen, J.; Yang, J. Global ammonia emissions from synthetic nitrogen fertilizer applications in agricultural systems: Empirical and process-based estimates and uncertainty. *Glob. Chang. Biol.* **2019**, *25*, 314–326. [CrossRef] [PubMed]
- Zhan, X.; Adalibieke, W.; Cui, X.; Winiwarter, W.; Reis, S.; Zhang, L.; Bai, Z.; Wang, Q.; Huang, W.; Zhou, F. Improved estimates of ammonia emissions from global croplands. *Environ. Sci. Technol.* **2021**, *55*, 1329–1338. [CrossRef]
- Sutton, M.A.; Reis, S.; Riddick, S.N.; Dragosits, U.; Nemitz, E.; Theobald, M.R.; Tang, Y.S.; Braban, C.F.; Vieno, M.; Dore, A.J.; et al. Towards a climate-dependent paradigm of ammonia emission and deposition. *Philos. Trans. R. Soc. B* **2013**, *368*. [CrossRef]
- Koerkamp, P.W.G.G.; Metz, J.H.M.; Uenk, G.H.; Phillips, V.R.; Holden, M.R.; Sneath, R.W.; Short, J.L.; White, R.P.; Hartung, J.; Seedorf, J.; et al. Concentrations and emissions of ammonia in livestock buildings in Northern Europe. *J. Agric. Eng. Res.* **1998**, *70*, 79–95. [CrossRef]
- Weerden van der, T.J.; Jarvis, S.C. Ammonia emission factors for nitrogen fertilisers applied to two contrasting grassland soils. *Environ. Pollut.* **1997**, *95*, 205–211. [CrossRef]
- Zhao, M.; Wang, S.; Tan, J.; Hua, Y.; Wu, D.; Hao, J. Variation of urban atmospheric ammonia pollution and its relation with PM_{2.5} chemical Property in winter of Beijing, China. *Aerosol Air Qual. Res.* **2016**, *16*, 1378–1389. [CrossRef]
- Huntzicker, J.J.; Cary, R.A.; Ling, C. Neutralization of sulfuric acid aerosol by ammonia. *Environ. Sci. Technol.* **1980**, *14*, 819–824. [CrossRef]
- Meng, Z.; Xu, X.; Lin, W.; Ge, B.; Xie, Y.; Song, B.; Jia, S.; Zhang, R.; Peng, W.; Wang, Y.; et al. Role of ambient ammonia in particulate ammonium formation at a rural site in the North China Plain. *Atmos. Chem. Phys.* **2018**, *18*, 167–184. [CrossRef]
- Wang, S.; Nan, J.; Shi, C.; Fu, Q.; Gao, S.; Wang, D.; Cui, H.; Saiz-Lopez, A.; Zhou, B. Atmospheric ammonia and its impacts on regional air quality over the megacity of Shanghai, China. *Sci. Rep.* **2015**, *5*, 15842. [CrossRef] [PubMed]
- Behera, S.N.; Sharma, M.; Aneja, V.P.; Balasubramanian, R. Ammonia in the atmosphere: A review on emission sources, atmospheric chemistry and deposition on terrestrial bodies. *Environ. Sci. Pollut. Res.* **2013**, *20*, 8092–8131. [CrossRef] [PubMed]
- Ye, X.; Ma, Z.; Zhang, J.; Du, H.; Chen, J.; Chen, H.; Yang, X.; Gao, W.; Geng, F. Important role of ammonia on haze formation in Shanghai. *Environ. Res. Lett.* **2011**, *6*, 2–7. [CrossRef]
- Chang, L.T.C.; Tsai, J.H.; Lin, J.M.; Huang, Y.S.; Chiang, H.L. Particulate matter and gaseous pollutants during a tropical storm and air pollution episode in Southern Taiwan. *Atmos. Res.* **2011**, *99*, 67–79. [CrossRef]
- Pinder, R.W.; Adams, P.J.; Pandis, S.N. Ammonia emission controls as a cost-effective strategy for reducing atmospheric particulate matter in the Eastern United States. *Environ. Sci. Technol.* **2007**, *41*, 380–386. [CrossRef] [PubMed]
- Krupa, S.V. Effects of atmospheric ammonia (NH₃) on terrestrial vegetation: A review. *Environ. Pollut.* **2003**, *124*, 179–221. [CrossRef]
- Bhattarai, G.; Lee, J.B.; Kim, M.H.; Ham, S.; So, H.S.; Oh, S.; Sim, H.J.; Lee, J.C.; Song, M.; Kook, S.H. Maternal exposure to fine particulate matter during pregnancy induces progressive senescence of hematopoietic stem cells under preferential impairment of the bone marrow microenvironment and aids development of myeloproliferative disease. *Leukemia* **2020**, *34*, 1481–1484. [CrossRef]
- Park, R.S.; Lee, S.; Shin, S.K.; Song, C.H. Contribution of ammonium nitrate to aerosol optical depth and direct radiative forcing by aerosols over East Asia. *Atmos. Chem. Phys.* **2014**, *14*, 2185–2201. [CrossRef]
- Xu, L.; Penner, J.E. Global simulations of nitrate and ammonium aerosols and their radiative effects. *Atmos. Chem. Phys.* **2012**, *12*, 9479–9504. [CrossRef]
- Sung, M.Y.; Park, J.S.; Lim, J.H.; Park, H.Y.; Cho, S.Y.A. Long term trend of gaseous and particulate acid/base species and effects of ammonia reduction on nitrate contained in PM_{2.5}. *J. Korean Soc. Atmos. Environ.* **2020**, *36*, 249–261. [CrossRef]
- Park, J.; Ryoo, J.; Jee, J.; Song, M. Origins and distributions of atmospheric ammonia in Jeonju during 2019–2020. *J. Korean Soc. Atmos. Environ.* **2020**, *36*, 2, 262–274. [CrossRef]

20. Chang, Y.; Zou, Z.; Zhang, Y.; Deng, C.; Hu, J.; Shi, Z.; Dore, A.J.; Collett, J.L. Assessing contributions of agricultural and nonagricultural emissions to atmospheric ammonia in a Chinese megacity. *Environ. Sci. Technol.* **2019**, *53*, 1822–1833. [CrossRef]
21. Zhou, C.; Zhou, H.; Holsen, T.M.; Hopke, P.K.; Edgerton, E.S.; Schwab, J.J. Ambient ammonia concentrations across New York State. *J. Geophys. Res. Atmos.* **2019**, *124*, 8287–8302. [CrossRef]
22. Huy, D.H.; Thanh, L.T.; Hien, T.T.; Noro, K.; Takenaka, N. Characteristics of ammonia gas and fine particulate ammonium from two distinct urban areas: Osaka, Japan, and Ho Chi Minh City, Vietnam. *Environ. Sci. Pollut. Res.* **2017**, *24*, 8147–8163. [CrossRef]
23. Phan, N.T.; Kim, K.H.; Shon, Z.H.; Jeon, E.C.; Jung, K.; Kim, N.J. Analysis of ammonia variation in the urban atmosphere. *Atmos. Environ.* **2013**, *65*, 177–185. [CrossRef]
24. Gong, L.; Lewicki, R.; Griffin, R.J.; Flynn, J.H.; Lefer, B.L.; Tittel, F.K. Atmospheric ammonia measurements in Houston, TX using an external-cavity quantum cascade laser-based sensor. *Atmos. Chem. Phys.* **2011**, *11*, 9721–9733. [CrossRef]
25. Pandolfi, M.; Amato, F.; Reche, C.; Alastuey, A.; Otjes, R.P.; Blom, M.J.; Querol, X. Summer ammonia measurements in a densely populated Mediterranean city. *Atmos. Chem. Phys.* **2012**, *12*, 7557–7575. [CrossRef]
26. Gupta, A.K.; Karar, K.; Ayoob, S.; John, K. Spatio-temporal characteristics of gaseous and particulate pollutants in an urban region of Kolkata, India. *Atmos. Res.* **2008**, *87*, 103–115. [CrossRef]
27. Lee, H.S.; Kang, C.M.; Kang, B.W.; Kim, H.K. Seasonal variations of acidic air pollutants in Seoul, South Korea. *Atmos. Environ.* **1999**, *33*, 3143–3152. [CrossRef]
28. Stelson, A.W.; Seinfeld, J.H. Thermodynamic prediction of the water activity, NH_4NO_3 dissociation constant, density and refractive index for the NH_4NO_3 – $(\text{NH}_4)_2\text{SO}_4$ – H_2O system at 25 °C. *Atmos. Environ.* **1982**, *16*, 2507–2514. [CrossRef]
29. Doyle, G.J.; Tuazon, E.C.; Graham, R.A.; Mischke, T.M.; Winer, A.M.; Pitts, J.N. Simultaneous concentrations of ammonia and nitric acid in a polluted atmosphere and their equilibrium relationship to particulate ammonium nitrate. *Environ. Sci. Technol.* **1979**, *13*, 1416–1419. [CrossRef]
30. Van Donkelaar, A.; Martin, R.V.; Li, C.; Burnett, R.T. Regional estimates of chemical composition of fine particulate matter using a combined geoscience-statistical method with information from satellites, models, and monitors. *Environ. Sci. Technol.* **2019**, *53*, 2595–2611. [CrossRef] [PubMed]
31. Gautam, S.; Patra, A.K.; Kumar, P. Status and chemical characteristics of ambient $\text{PM}_{2.5}$ pollutions in China: A review. *Environ. Dev. Sustain.* **2019**, *21*, 1649–1674. [CrossRef]
32. Li, Y.J.; Sun, Y.; Zhang, Q.; Li, X.; Li, M.; Zhou, Z.; Chan, C.K. Real-time chemical characterization of atmospheric particulate matter in China: A review. *Atmos. Environ.* **2017**, *58*, 270–304. [CrossRef]
33. Cheng, Z.; Luo, L.; Wang, S.; Wang, Y.; Sharma, S.; Shimadera, H.; Wang, X.; Bressi, M.; de Miranda, R.M.; Jiang, J.; et al. Status and characteristics of ambient $\text{PM}_{2.5}$ pollution in global megacities. *Environ. Int.* **2016**, *89–90*, 212–221. [CrossRef] [PubMed]
34. Philip, S.; Martin, R.V.; Van Donkelaar, A.; Lo, J.W.H.; Wang, Y.; Chen, D.; Zhang, L.; Kasibhatla, P.S.; Wang, S.; Zhang, Q.; et al. Global chemical composition of ambient fine particulate matter for exposure assessment. *Environ. Sci. Technol.* **2014**, *48*, 13060–13068. [CrossRef]
35. Guo, W.; Zheng, N.; Zhang, Z. Stable nitrogen isotopic signatures reveal the NH_4^+ evolution processes in pollution episodes in urban southwestern China. *Atmos. Res.* **2021**, *253*, 105474. [CrossRef]
36. Saraswati; Sharma, S.K.; Saxena, M.; Mandal, T.K. Characteristics of gaseous and particulate ammonia and their role in the formation of secondary inorganic particulate matter at Delhi, India. *Atmos. Res.* **2019**, *218*, 34–49. [CrossRef]
37. Ge, B.; Xu, X.; Ma, Z.; Pan, X.; Wang, Z.; Lin, W.; Ouyang, B.; Xu, D.; Lee, J.; Zheng, M.; et al. Role of ammonia on the feedback between AWC and inorganic aerosol formation during heavy pollution in the North China Plain. *Earth Space Sci.* **2019**, *6*, 1675–1693. [CrossRef]
38. Meng, Z.; Lin, W.; Zhang, R.; Han, Z.; Jia, X. Summertime ambient ammonia and its effects on ammonium aerosol in urban Beijing, China. *Sci. Total Environ.* **2017**, *579*, 1521–1530. [CrossRef]
39. Edgerton, E.S.; Saylor, R.D.; Hartsell, B.E.; Jansen, J.J.; Alan Hansen, D. Ammonia and ammonium measurements from the southeastern United States. *Atmos. Environ.* **2007**, *41*, 3339–3351. [CrossRef]
40. Gao, J.; Wei, Y.; Shi, G.; Yu, H.; Zhang, Z.; Song, S.; Wang, W.; Liang, D.; Feng, Y. Roles of RH, aerosol pH and sources in concentrations of secondary inorganic aerosols, during different pollution periods. *Atmos. Environ.* **2020**, *241*, 117770. [CrossRef]
41. Wu, Z.; Wang, Y.; Tan, T.; Zhu, Y.; Li, M.; Shang, D.; Wang, H.; Lu, K.; Guo, S.; Zeng, L.; et al. Aerosol liquid water driven by anthropogenic inorganic salts: Implying its key role in haze formation over the North China Plain. *Environ. Sci. Technol. Lett.* **2018**, *5*, 160–166. [CrossRef]
42. Nguyen, T.K.V.; Zhang, Q.; Jimenez, J.L.; Pike, M.; Carlton, A.G. Liquid water: Ubiquitous contributor to aerosol mass. *Environ. Sci. Technol. Lett.* **2016**, *3*, 257–263. [CrossRef]
43. Picarro Inc. G2103 Analyzer Datasheet—G2103-DS20-V1.2-AHDS-190917. 2019. Available online: <http://www.picarro.com> (accessed on 1 November 2021).
44. Pogány, A.; Balslev-Harder, D.; Braban, C.F.; Cassidy, N.; Ebert, V.; Ferracci, V.; Hieta, T.; Leuenberger, D.; Martin, N.A.; Pascale, C.; et al. A metrological approach to improve accuracy and reliability of ammonia measurements in ambient air. *Meas. Sci. Technol.* **2016**, *27*, 115012. [CrossRef]
45. Yao, L.; Kong, S.; Zheng, H.; Chen, N.; Zhu, B.; Xu, K.; Cao, W.; Zhang, Y.; Zheng, M.; Cheng, Y.; et al. Co-benefits of reducing $\text{PM}_{2.5}$ and improving visibility by COVID-19 lockdown in Wuhan. *Clim. Atmos. Sci.* **2021**, *4*, 40. [CrossRef]

46. Wang, X.; Zhang, R.; Yu, W. The Effects of PM_{2.5} Concentrations and Relative Humidity on Atmospheric Visibility in Beijing. *J. Geophys. Res. Atmos.* **2019**, *124*, 2235–2259. [\[CrossRef\]](#)
47. Byun, D.; Schere, K.L. Review of the Governing Equations, Computational Algorithms, and Other Components of the Models-3 Community Multiscale Air Quality (CMAQ) Modeling System. *Appl. Mech. Rev.* **2006**, *59*, 51–77. [\[CrossRef\]](#)
48. Skamarock, W.C.; Klemp, J.B. A time-split nonhydrostatic atmospheric model for weather research and forecasting applications. *J. Comput. Phys.* **2008**, *227*, 3465–3485. [\[CrossRef\]](#)
49. Benjey, W.; Houyox, M.; Susick, J. Implementation of the SMOKE Emission Data Processor and SMOKE Tool Input Data Processor in Models-3. In Proceedings of the Emission Inventory Conference, Denver, CO, USA, 1–4 May 2001; Available online: <https://cfpub.epa.gov> (accessed on 20 November 2021).
50. Park, R.J.; Oak, Y.J.; Emmons, L.K.; Kim, C.H.; Pfister, G.G.; Carmichael, G.R.; Saide, P.E.; Cho, S.-Y.; Kim, S.; Woo, J.-H.; et al. Multi-model intercomparisons of air quality simulations for the KORUS-AQ campaign. *Elementa* **2021**, *9*. [\[CrossRef\]](#)
51. Woo, J.-H.; Kim, Y.; Kim, J.; Park, M.; Jang, Y.; Kim, J.; Bu, C.; Lee, Y.; Park, R.; Oak, Y.; et al. KORUS Emissions: A comprehensive Asian emissions information in support of the NASA/NIER KORUS-AQ mission. *Elementa*. **2021**, in press.
52. Clean Air Policy Support System (CAPSS). 2017 Korea National Air Pollutants Emission. 2019. Available online: <https://airemiss.nier.go.kr> (accessed on 1 May 2021).
53. Burr, M.J.; Zhang, Y. Source apportionment of fine particulate matter over the Eastern US, Part I: Source sensitivity simulations using CMAQ with the Brute Force method. *Atmos. Pollut. Res.* **2011**, *2*, 300–317. [\[CrossRef\]](#)
54. Kim, H.C.; Kim, E.; Bae, C.; Hoon Cho, J.; Kim, B.U.; Kim, S. Regional contributions to particulate matter concentration in the Seoul metropolitan area, South Korea: Seasonal variation and sensitivity to meteorology and emissions inventory. *Atmos. Chem. Phys.* **2017**, *17*, 10315–10332. [\[CrossRef\]](#)
55. Kim, E.; Kim, B.U.; Kim, H.C.; Kim, S. Sensitivity of fine particulate matter concentrations in South Korea to regional ammonia emissions in Northeast Asia. *Environ. Pollut.* **2021**, *273*, 116428. [\[CrossRef\]](#) [\[PubMed\]](#)
56. Bae, M.; Kim, B.U.; Kim, H.C.; Kim, S. A multiscale tiered approach to quantify contributions: A case study of PM_{2.5} in South Korea during 2010–2017. *Atmosphere* **2020**, *11*, 141. [\[CrossRef\]](#)
57. Li, X.; Zhang, Q.; Zhang, Y.; Zheng, B.; Wang, K.; Chen, Y.; Wallington, T.J.; Han, W.; Shen, W.; Zhang, X. Source contributions of urban PM_{2.5} in the Beijing–Tianjin–Hebei region: Changes between 2006 and 2013 and relative impacts of emissions and meteorology. *Atmos. Environ.* **2015**, *123*, 229–239. [\[CrossRef\]](#)
58. Zhang, Z.; Wang, W.; Cheng, M.; Liu, S.; Xu, J.; He, Y.; Meng, F. The contribution of residential coal combustion to PM_{2.5} pollution over China's Beijing–Tianjin–Hebei region in winter. *Atmos. Environ.* **2017**, *159*, 147–161. [\[CrossRef\]](#)
59. Zbieranowski, A.L.; Aherne, J. Ambient concentrations of atmospheric ammonia, nitrogen dioxide and nitric acid across a rural–urban–agricultural transect in southern Ontario, Canada. *Atmos. Environ.* **2012**, *62*, 481–491. [\[CrossRef\]](#)
60. Dammers, E.; Schaap, M.; Haaima, M.; Palm, M.; Kruit, R.J.W.; Volten, H.; Hensen, A.; Swart, D.; Erisman, J.W. Measuring atmospheric ammonia with remote sensing campaign: Part 1—Characterisation of vertical ammonia concentration profile in the centre of The Netherlands. *Atmos. Environ.* **2017**, *169*, 97–112. [\[CrossRef\]](#)
61. Zöll, U.; Brümmer, C.; Schrader, F.; Ammann, C.; Ibrom, A.; Flechard, C.R.; Nelson, D.D.; Zahniser, M.; Kutsch, W.L. Surface-atmosphere exchange of ammonia over peatland using QCL-based eddy-covariance measurements and inferential modelling. *Atmos. Chem. Phys.* **2016**, *16*, 11283–11299. [\[CrossRef\]](#)
62. Oh, S.; Kim, S.; Lee, J.; Park, J.; Jee, J.; Hong, S.; Kwon, K.; Song, M. Spatial distributions of atmospheric ammonia in a rural area in south Korea and the associated impact on a nearby urban area. *Atmosphere* **2021**, *12*, 1411. [\[CrossRef\]](#)
63. Jo, G.; Kim, D.; Song, M. PM_{2.5} Concentrations and Chemical Compositions in Jeonju from 2017 to 2018. *J. Korean Soc. Atmos. Environ.* **2018**, *34*, 876–888. [\[CrossRef\]](#)
64. Mutuku, K.J.; Lee, Y.Y.; Chang-Chien, G.P.; Lin, S.L.; Chen, W.H.; Hou, W.C. Chemical fingerprints for PM_{2.5} in the ambient air near a raw material storage site for iron ore, coal, limestone, and sinter. *Aerosol Air Qual. Res.* **2021**, *21*, 1–17. [\[CrossRef\]](#)
65. Ricciardelli, I.; Bacco, D.; Rinaldi, M.; Bonafè, G.; Scotto, F.; Trentini, A.; Bertacci, G.; Ugolini, P.; Zigola, C.; Rovere, F.; et al. A three-year investigation of daily PM_{2.5} main chemical components in four sites: The routine measurement program of the Supersito Project (Po Valley, Italy). *Atmos. Environ.* **2017**, *152*, 418–430. [\[CrossRef\]](#)
66. Cao, J.J.; Shen, Z.X.; Chow, J.C.; Watson, J.G.; Lee, S.C.; Tie, X.X.; Ho, K.F.; Wang, G.H.; Han, Y.M. Winter and Summer PM_{2.5} Chemical Compositions in Fourteen Chinese Cities. *J. Air Waste Manag. Assoc.* **2012**, *62*, 1214–1226. [\[CrossRef\]](#)
67. WHO (World Health Organization). *Air Quality Guidelines: Global Update 2005*; WHO: Geneva, Switzerland, 2006; Available online: <https://wedocs.unep.org/20.500.11822/8712> (accessed on 20 November 2021).
68. Hu, G.; Zhang, Y.; Sun, J.; Zhang, L.; Shen, X.; Lin, W.; Yang, Y. Variability, formation and acidity of water-soluble ions in PM_{2.5} in Beijing based on the semi-continuous observations. *Atmos. Res.* **2014**, *145–146*, 1–11. [\[CrossRef\]](#)
69. Seinfeld, J.; Pandis, S. *Atmospheric Chemistry and Physics: From Air Pollution to Climate Change*, 3rd ed.; Wiley: Hoboken, NJ, USA, 2016; ISBN 978-1-118-94740-1.
70. Pinder, R.W.; Dennis, R.L.; Bhawe, P.V. Observable indicators of the sensitivity of PM_{2.5} nitrate to emission reductions—Part I: Derivation of the adjusted gas ratio and applicability at regulatory-relevant time scales. *Atmos. Environ.* **2008**, *42*, 1275–1286. [\[CrossRef\]](#)
71. Winston, P.W.; Bates, D.H. Saturated solutions for the control of humidity in biological research. *Ecology* **1960**, *41*, 232–237. [\[CrossRef\]](#)

-
72. Kim, E.; Kim, B.U.; Kim, H.C.; Kim, S. Direct and cross impacts of upwind emission control on downwind PM_{2.5} under various NH₃ conditions in Northeast Asia. *Environ. Pollut.* **2021**, *268*, 115794. [[CrossRef](#)]
 73. Kumar, N.; Park, R.J.; Jeong, J.I.; Woo, J.H.; Kim, Y.; Johnson, J.; Yarwood, G.; Kang, S.; Chun, S.; Knipping, E. Contributions of International Sources to PM_{2.5} in South Korea. *Atmos. Environ.* **2021**, 118542. [[CrossRef](#)]
 74. Bae, C.; Kim, B.U.; Kim, H.C.; Yoo, C.; Kim, S. Long-range transport influence on key chemical components of PM_{2.5} in the Seoul Metropolitan Area, South Korea, during the years 2012–2016. *Atmosphere* **2020**, *11*, 48. [[CrossRef](#)]
 75. Zhu, L.; Henze, D.K.; Bash, J.O.; Cady-Pereira, K.E.; Shephard, M.W.; Luo, M.; Capps, S.L. Sources and impacts of atmospheric NH₃: Current understanding and frontiers for modeling, measurements, and remote sensing in North America. *Curr. Pollut. Rep.* **2015**, *1*, 95–116. [[CrossRef](#)]
 76. Galperin, M.V.; Sofiev, M.A. The long-range transport of ammonia and ammonium in the Northern Hemisphere. *Atmos. Environ.* **1998**, *32*, 373–380. [[CrossRef](#)]